optica

On-chip optical tweezers based on freeform optics

Shaoliang Yu,[1,†,*] Jinsheng Lu,[2,3,†] Vincent Ginis,[2,4] Simon Kheifets,[2] Soon Wei Daniel Lim,[2] Min Qiu,[5] Tian Gu,[6] Juejun Hu,[1,6,7] and Federico Capasso[2,8]

[1]Department of Materials Science and Engineering, Massachusetts Institute of Technology, Cambridge, Massachusetts 02139, USA
[2]Harvard John A. Paulson School of Engineering and Applied Sciences, Harvard University, Cambridge, Massachusetts 02138, USA
[3]State Key Laboratory of Modern Optical Instrumentation, College of Optical Science and Engineering, Zhejiang University, Hangzhou, 310027, China
[4]Data Lab/Applied Physics, Vrije Universiteit Brussel, 1050 Brussels, Belgium
[5]Key Laboratory of 3D Micro/Nano Fabrication and Characterization of Zhejiang Province, School of Engineering, Westlake University, Hangzhou, 310024, China
[6]Materials Research Laboratory, Massachusetts Institute of Technology, Cambridge, Massachusetts 02139, USA
[7]e-mail: hujuejun@mit.edu
[8]e-mail: capasso@seas.harvard.edu
*Corresponding author: yusl@mit.edu

Received 5 January 2021; revised 15 February 2021; accepted 18 February 2021 (Doc. ID 418837); published 12 March 2021

Since its advent in the 1970s, optical tweezers have been widely deployed as a preferred non-contact technique for manipulating microscale objects. On-chip integrated optical tweezers, which afford significant size, weight, and cost benefits, have been implemented, relying upon near-field evanescent waves. As a result, these tweezers are only capable of manipulation in near-surface regions and often demand high power since the evanescent interactions are relatively weak. We introduce on-chip optical tweezers based on freeform micro-optics, which comprise optical reflectors or refractive lenses integrated on waveguide end facets via two-photon polymerization. The freeform optical design offers unprecedented degrees of freedom to design optical fields with strong three-dimensional intensity gradients, useful for trapping and manipulating suspended particles in an integrated chip-scale platform. We demonstrate the design, fabrication, and measurement of both reflective and refractive micro-optical tweezers. The reflective tweezers feature a remarkably low trapping threshold power, and the refractive tweezers are particularly useful for multiparticle trapping and interparticle interaction analysis. Our integrated micro-optical tweezers uniquely combine a compact footprint, broadband operation, high trapping efficiency, and scalable integration with planar photonic circuits. This class of tweezers is promising for on-chip sensing, cell assembly, particle dynamics analysis, and ion trapping.

https://doi.org/10.1364/OPTICA.418837

1. INTRODUCTION

Following the first experimental demonstration by Arthur Ashkin [1], optical trapping has become the technology of choice for non-contact manipulation of microscopic objects, with far-reaching impacts on applications ranging from biomechanical characterization to sorting of colloidal particles [2–15]. Conventional optical tweezers use high-numerical-aperture (NA) lenses to generate a stable gradient trapping potential [2], which entails bulky, costly benchtop instruments. As an alternative, optical fiber-based tweezers have also been realized in the form of two counter aligned fibers or a lensed/tapered fiber [16–24]. However, both approaches offer limited control over the optical field, and they are not amenable to large-scale on-chip integration critical to applications such as optical sorting and ion trapping in the context of quantum computing [7].

To resolve this challenge, planar photonic devices such as optical waveguides [25–31], plasmonic structures [32–35], and optical resonators [36–42] have been proposed for on-chip trapping. These devices rely on evanescent waves to produce the optical gradient potential, which only allows 2D particle manipulation in the immediate proximity of the chip surface due to the very short (hundreds of nanometers) decay length of evanescent fields.

In this paper, we demonstrate a new class of on-chip optical tweezers whose functionality is based on waveguide-integrated, freeform micro-optical elements. Freeform optics opens up a large design space for optical wavefront control and has been regarded as a disruptive optical systems technology. However, the development of freeform optics in their bulk incarnation has been hampered by the fabrication challenges of free surface shaping with subwavelength accuracy. Recent developments in two-photon polymerization (TPP) [43], a process capable of on-demand printing of three-dimensional (3D) structures with critical dimensions well below the classical diffraction limit, have opened up a promising route for scalable fabrication of freeform optics—with a miniature form factor amenable to on-chip integration [44–46]. We show that freeform micro-optical elements are ideally suited for on-chip optical tweezers benefitting from

several unique features. First, this design enables precise positioning of the trap location in the 3D region above the chip and facile adaptations of the trapping potential. Second, the micro-optics are seamlessly integrated with on-chip waveguides and can be readily interfaced with photonic integrated circuits to impart new functionalities such as dynamic tuning and switching of optical traps. In addition, compared to other planar devices that can also be used for free-space outcoupling such as diffractive gratings, plasmonic scatterers, and metasurfaces, freeform reflective or refractive micro-optics offer excellent optical efficiency (>95% efficiency from the waveguide to the focal spot) and broadband operation [46]. The high efficiency facilitates a low trapping threshold power, whereas the large spectral bandwidth is useful for quantum state preparation and fluorescence or Raman excitation. Finally, the waveguides can further function as integrated optical monitors, providing real-time information about the motion of trapped particles through the measurement of the backscattered light intensity [20]. In the following, we will present the design, fabrication, and characterization of two embodiments of the on-chip tweezers based on reflective and refractive micro-optics.

2. TRAPPING WITH FOCUSING REFLECTORS

A. Design and Modeling

In this section, we describe the design and modeling of on-chip optical tweezers based on freeform reflectors. The basic concept is to use a pair of freeform reflectors attached to the end facets of waveguides to redirect and focus light to a predefined spot above the chip through total internal reflection (TIR) as shown in Fig. 1(a). Specifically, we use two ellipsoidal reflectors to focus the counterpropagating light output from two waveguides to the same point. The focused beams intersect with an optimized angle to generate a 3D gradient field for particle trapping in a way similar to a dark-field objective [Fig. 1(b)]. The ellipsoidal reflectors are designed such that one of the foci coincides with the waveguide output and the other with the trap location as indicated in Fig. 1(c). The structure was further optimized by slightly offsetting the elliptical reflector along the longitudinal direction of the waveguide, where the amount of offset is determined by full-wave simulations [47].

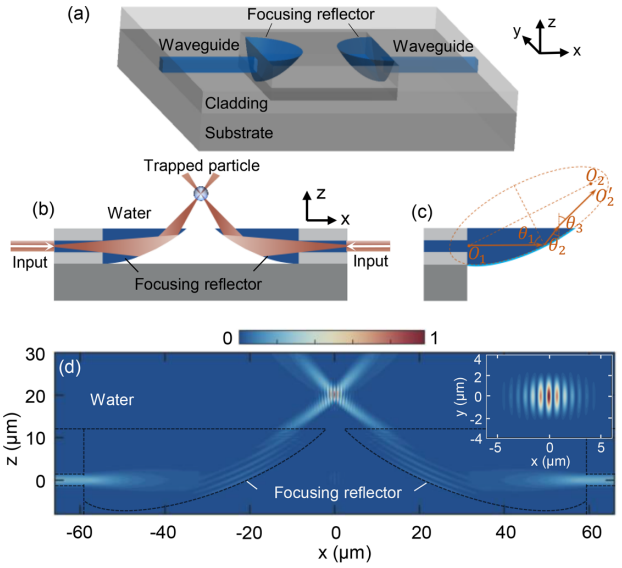

Fig. 1. On-chip optical trapping using freeform focusing reflectors. (a) A 3D schematic layout of the chip. (b) $x-z$ cross section of the device illustrating particle trapping at the intersection of two focused beams. (c) The design of the focusing reflectors. (d) FDTD simulated intensity distribution for the transverse-electric (TE) mode at the cross section along the center plane ($x-z$) of the waveguide. The black dashed lines indicate the profiles of the devices. The inset shows the intensity distribution on the $x-y$ plane at the focal spot (z = 20 μm).

In this demonstration, we used single-mode polymer waveguides with a core size of 2.5 μm × 2.5 μm, with the mode profile shown in Fig. S1. The core and cladding materials are EpoCore and OrmoCore (Micro Resist Technology GmbH) with refractive indices $n_{core} = 1.575$ and $n_{clad} = 1.537$, respectively. To eliminate Fresnel reflection at the waveguide facet, EpoCore is also used as the reflector material. The waveguide design yields a divergence angle of the beam output of approximately 10°. To ensure TIR at the reflector–water interface, the angles θ_1 and θ_3 must meet the conditions $56.6° < \theta_1 < 73.3°$ and $28.3° < \theta_3 < 90°$ [Fig. 1(c)], assuming that the refractive index of water at the 1550 nm trapping wavelength is $n_{water} = 1.315$. In our design, the chief ray direction is given by $\theta_1 = 65°$ and $\theta_3 = 50°$, corresponding to an equivalent NA of 1.0 ($= n_{water} \cdot \sin\theta_3$) in water for the crossing beams.

Figure 1(d) depicts the optical intensity distribution on the center cross-sectional plane ($x-z$) of the waveguide for the transverse-electric (TE) polarized mode, simulated using 3D finite-difference time-domain (FDTD). In this example, the beam's focal spot is set to be 8 μm above the chip surface. The $x-y$-plane intensity distribution is shown in the inset of Fig. 1(d). The focal spot full widths at half-maximum (FWHM) in the x, y and z directions are 1.9, 2.1, and 2.5 μm, respectively.

A microparticle in this focal spot region experiences a conservative optical gradient force and a nonconservative optical scattering force. In the y direction, the optical scattering force is negligible since Poynting vectors of the incident beams lie within the $x-z$ plane. In the x direction, a standing wave is formed [inset of Fig. 1(d)], and the scattering forces from the two beams cancel out. Therefore, the optical forces in the x and y directions are dominated by the conservative gradient force, which form the trapping potential for a microparticle. However, in the z direction, the scattering force cannot be neglected and tends to propel the microparticle away from the trap. Considering the fact that the gradient force originating from the strong light intensity gradient is dominant in the z direction for our case, we can define an effective potential depth by restricting our analysis to the z direction [48]. The calculated optical forces and trapping potentials of a 4.5 μm diameter polystyrene sphere ($n = 1.56$) in water are presented in Fig. 2. The modes in both waveguides are TE polarized and in phase. Interference between the two beams occurs at the focal spot where they cross, resulting in spatially varying intensity fringes, shown in Fig. 2(a). In Figs. 2(b)–2(d) we plot the optical force and trapping potential versus displacement from the equilibrium position, both normalized to the total power sent into the two waveguides. The optical forces are calculated with the Maxwell stress tensor (MST) method. Maximum forces of 1.0, 1.0, and 1.2 pN/mW are obtained along the x, y, and z directions, corresponding to trapping potential depths of 519, 574, and 330 k_BT/mW, respectively, where k_B denotes the Boltzmann constant and T represents temperature. By fitting the simulated trapping potential with a harmonic well (Fig. S2), theoretically expected trapping stiffnesses can be obtained along the x, y, and z directions as 0.23, 0.67, and 0.39 pN/μm/mW, respectively. In water, Brownian motion, with an average kinetic energy of

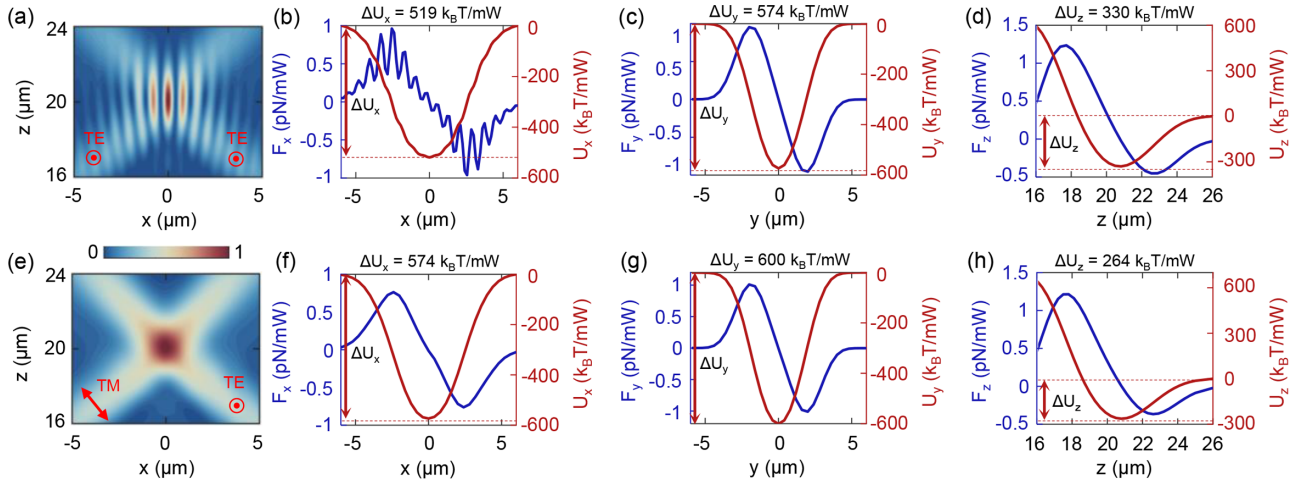

Fig. 2. Numerical simulations of optical forces and trapping potentials for the focusing reflector-based optical tweezers. (a)–(d) Simulated (a) intensity distribution at the focal spot and (b)–(d) optical forces and trapping potentials along the x, y, and z directions when the waveguide output modes are both TE polarized and in phase. (e)–(h) Simulated (e) intensity distribution, (f)–(h) optical forces, and trapping potentials along the x, y, and z directions when the waveguide output modes have orthogonal polarization. The simulations are normalized to the total power sent into the two waveguides.

1.5 k_BT, will randomly drive the particle to diffuse out of the trap. To achieve stable trapping, a minimum potential depth of 10 k_BT is usually defined as a trapping threshold [2]. The 10 k_BT stability threshold corresponds to trapping powers down to 19 μW (x), 17 μW (y), and 30 μW (z) in our design. These threshold power values are much lower than previous reports of on-chip optical tweezers [27,49], benefitting from the high optical coupling efficiency and optimized 3D field profile produced by the micro-optics. We also note that the two beams' shallow incidence contributes to the reduction of the force due to radiation pressure along the z direction and therefore stabilizes trapping compared to a conventional high-NA objective. To further demonstrate this point, we simulated the same particle trapped by a single Gaussian beam with NA = 1.0 (Fig. S3) and found that the potential depth along the z direction is 137 k_BT/mW, 60% less than our design.

In the simulations, we assume that the output beams from the two waveguides have identical polarization, phase, and power. To investigate the robustness of the device operation to structure variations, we consider the extreme scenarios where the two beams have orthogonal polarizations [Figs. 2(e)–2(h)], 10% of power fluctuation (Figs. S4a–S4e), and a π phase difference (Figs. S4f–S4j). The nearly identical optical forces and potential depths along all three axes suggest insensitivity of the device performance to polarization, power, and phase changes. The result shows that the optical tweezer design is inherently tolerant against fabrication variations.

B. Experimental Characterizations

The fabrication process is schematically illustrated in Fig. S5, with details and parameters described in Supplement 1. The waveguide was patterned with an i-line UV stepper (GCA AutoStep 200) on top of a 10 μm thick bottom cladding layer, followed by spin coating of the top cladding layer with 10 μm thickness. A trench with a lateral dimension of 120 μm × 40 μm and a depth of 18 μm was then etched into the bottom cladding layers via reactive-ion etching (RIE) to define the waveguide output facets to which the reflectors are attached. The freeform reflectors were then sculpted using TPP in the photosensitive polymer EpoCore with a Photonic Professional GT 3D printer station (Nanoscribe GmbH). The 3D structures for TPP process of the focusing reflectors can be found in Visualization 1 and Fig. S6. The fabricated device is displayed in Fig. 4(a) and Fig. S7. Light coupled into the chip was first split into two equal parts by a Y-branch and then directed to the two waveguide ports of the tweezers.

The setup used to measure the focal spot's light intensity profile and characterize the trapping performance is depicted in Fig. 3(a). A liquid chamber was assembled on the chip using a coverslip and was filled with an aqueous microparticle solution. A 1550 nm wavelength laser was coupled into the chip by a lensed fiber via edge coupling. To map the intensity profile near the focal spot, the position of the 63× objective was swept along the out-of-plane (z) direction using a piezoelectric motor, and a series of images, each representing the in-plane intensity distribution at one z position,

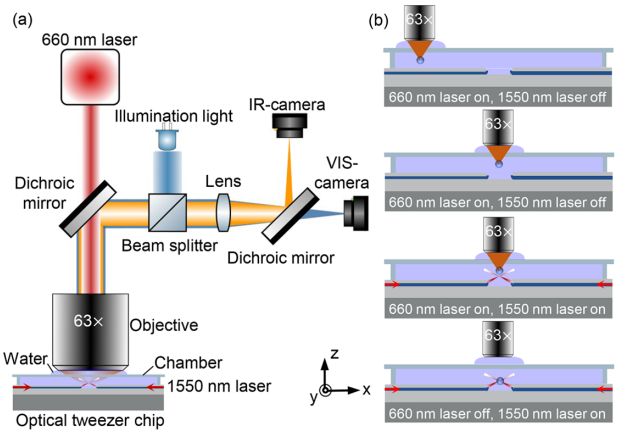

Fig. 3. Schematic of the experimental setup used to demonstrate on-chip trapping, map the focal spot profile, and measure the trapping strength of the on-chip optical tweezers. (a) A 660 nm laser beam, focused through an oil-immersion 63× objective, brings a particle to the trapping location. The particle's position is visualized using light collected through the oil-immersion lens and focused onto the VIS-camera and IR-camera. (b) An illustration of the procedure used to transfer a particle from a conventional microscope optical trap (660 nm laser) to the on-chip trap (1550 nm laser).

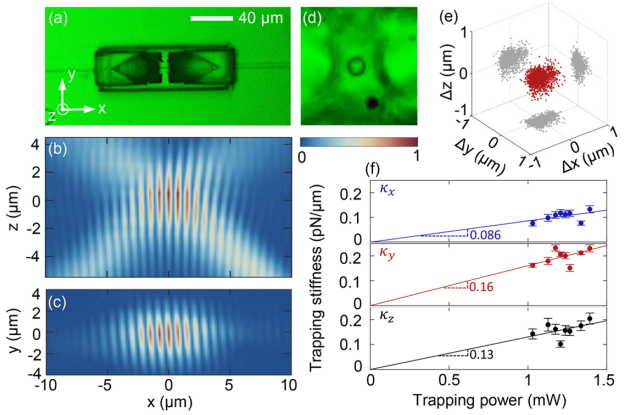

Fig. 4. Experimental measurements of the optical trap characteristics. (a) Top view optical microscope image of two focusing reflectors on the chip. (b), (c) Cross sections of the measured light intensity distribution through the focus of the two beams on the (b) $x-z$ plane (y = 0) and (c) $x-y$ plane. (d) Optical microscope image of a particle trapped by the chip. The diameter of the trapped particle is 4.5 μm. (e) Individual measurements of the particle's location (red dots) in 3D space over a 4 min period under a laser power of 1.39 mW, along with its projection onto each orthogonal plane (grey dots). (f) Extracted trapping stiffness along the x, y, and z directions versus laser power.

was captured by an IR camera (Visualization 2). The 3D intensity distribution was then reconstructed, as shown in Fig. 4(b) ($x-z$ plane cut) and Fig. 4(c) ($x-y$ plane cut across the focal spot center). The measured focal spot FWHM is approximately 5.7 μm (x) × 2.8 μm (y) × 4.3 μm (z). The increased spot size compared with the simulated results is attributed to deviation of the reflector shape from the design caused by volume change during polymer cross-linking.

A conventional microscope optical tweezer with a water-immersed objective and 660 nm wavelength laser was used to move a particle to the on-chip trap [Fig. 3(b)]. After turning off the 660 nm laser and turning on the 1550 nm laser, the particle can be trapped stably near the focal spot of the two reflectors as shown in Fig. 4(d). To confirm successful trapping, the 1550 nm laser was switched off and on multiple times. When the laser was off, the sphere drifted away from the trap due to Brownian motion. The particle was recaptured by the trap after the laser was switched on (Visualization 3). Its spatial positions were extracted from the recorded video by fitting the position and diameter of the captured particle as shown in Fig. S8. The displacement of the trapped particle from its equilibrium position during a 4 min measurement is plotted in Fig. 4(e) (Visualization 4). The data imply that the particle is better confined along the y and z directions than in the x direction, consistent with the field distribution along the three directions. Traping stiffness is estimated by fitting the displacement distribution with a Gaussian function under different laser powers, which yields 0.09 ± 0.01, 0.16 ± 0.02, and 0.13 ± 0.02 pN/μm/mW along the x, y, and z directions, respectively [Fig. 4(f)].

3. TRAPPING WITH REFRACTIVE MICROLENSES

In this section, we demonstrate that refractive micro-optics can similarly be applied to on-chip optical trapping. The refractive optical tweezers consist of two microlenses with a Cartesian oval shape (Visualization 5, Fig. S9). Considering the waveguide beam as a pointlike source, the shape of the lens can be determined by seeking a constant optical path length between the pointlike source and the target focal spot [50]. The lenses are attached to the output facets of two waveguides facing each other [Fig. 5(a)]. The counterpropagating beams exiting from the waveguides are focused to the same spot by the microlenses to form a trap. The shape of the trap can be readily controlled by changing the lenses' focusing power: tightly focused beams lead to strong confinement along the longitudinal direction, whereas lower-NA microlenses lead to extended traps along the x direction. In our experiment, we designed an elongated trap shape suitable for multiparticle trapping: the beam is tightly localized in the transverse $y-z$ plane and only loosely confined along the longitudinal x direction. The optical intensity distribution corresponds to a FWHM spot size of 12.2 μm (x) × 1.6 μm (y) × 1.6 μm (z). This intensity profile creates a single stable trap site in the $y-z$ plane while permitting multiple particles to be simultaneously trapped along the longitudinal x direction (Fig. S10).

We experimentally validated dual particle trapping using the microlens-based tweezers [Fig. 5(c), Visualization 6], which can serve as a simple platform for investigating the interactions between the two particles. Figure 5(d) plots the statistical distribution of the relative displacement between the two trapped particles measured over a 5 min period, with the corresponding probability distribution functions (PDFs) of D_x and D_y (relative displacement along the x and y directions, respectively), shown in Figs. 5(e) and 5(f). The histograms reveal that D_y follows a Gaussian distribution due to the single trapping site defined by the transverse optical confinement. In contrast, the dispersion of D_x cannot be accurately described with a Gaussian distribution. To elucidate this observation, we consider two types of interactions acting along the longitudinal x direction: the optical attractive force coming from both the radiation pressure force and the gradient force, which attracts the particles toward each other, and the counteracting double-layer repulsive force [51]. The probability distributions of D_x and D_y are given by $\mathrm{p}(D_i) = Ce^{-\frac{U(D_i)}{k_B T}}$, where $U(D_i)$ is the potential energy. Here the index i takes value x or y. The potential energy (per unit optical power) along the y direction is a harmonic potential $U(D_y) = \frac{1}{2}\kappa_y D_y^2$, where κ_y is the trap stiffness. The potential energy in the x direction follows $U(D_x) = Ce^{-\kappa(D_x - D_{x,m})} + F_{\mathrm{attr}}(D_x - D_{x,m})$, where κ is the Debye parameter and $D_{x,m}$ gives the interparticle spacing when the potential energy is minimum. By fitting the model with the experiment data, we obtain $\kappa_y = 8.27\ \mathrm{k_B T/\mu m^2} = 0.033\ \mathrm{pN/\mu m}$, $\kappa = 3.26\ \mu\mathrm{m}^{-1}$, $D_{x,m} = 5.11$ μm, and $F_{\mathrm{attr}} = 32.29\ \mathrm{k_B T/\mu m} = 0.13$ pN. This model fit is in agreement with the measured results as illustrated in Figs. 5(e)–5(h).

An added benefit of the on-chip micro-optical tweezers is that light backscattered into the feeding waveguides can also be employed to monitor the movement of the trapped particles in real time [20]. Taking the refractive optical tweezers as an example, displacement of the particle from its equilibrium position along the x direction breaks the mirror symmetry and induces a large difference in reflected light intensity received by the two waveguides. Our FDTD simulation results suggest that the particle displacement can lead to a reflection difference as large as 25% (Fig. S11), which offers a convenient technique for monitoring the motion of the trapped particle with high precision.

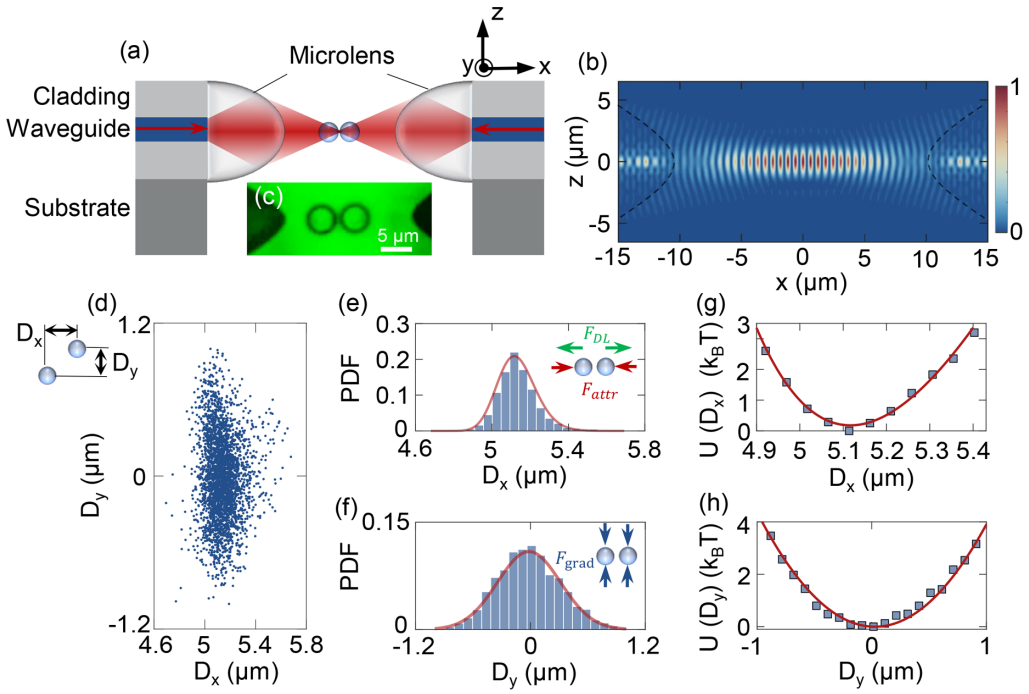

Fig. 5. Refractive micro-optical tweezer characterization. (a) Schematic depicting trapping of two particles by the refractive micro-optical tweezers. (b) Simulated optical intensity distribution in the region between two microlenses. The black lines mark the profiles of the microlenses. (c) Optical microscope image of two particles simultaneously trapped by the device. (d) The measured center-to-center displacement between the two trapped particles in the x and y directions. Three thousand experimental data points were collected over a 5 min measurement duration. (e), (f) Extracted probability distribution histograms of the x and y spacings between the particles. The optical attractive force between the particles F_{attr}, double-layer repulsion force F_{DL}, and optical gradient force F_{grad} are schematically illustrated as an inset. (g), (h) Potential energy profiles along the x and y directions computed from the data in (e), (f). The red curves in (e)–(h) are theoretical predictions based on our particle interaction model.

4. CONCLUSION

In summary, we proposed and experimentally validated freeform micro-optics-based optical tweezers as a new platform for on-chip trapping and manipulation. Leveraging the ability to shape the free-space wavefront on demand by freeform micro-optics, we show that 3D gradient optical fields can be created and engineered to trap one or multiple suspended particles using a chip-scale platform. Reflective and refractive micro-optical designs enabling low trapping power and interparticle interaction analysis were demonstrated. The micro-optical tweezers uniquely combine versatile configuration, high optical efficiency, compact footprint, broadband operation, and integration scalability, qualifying it as a promising platform for a plethora of applications such as on-chip sensing, cell analysis and assembly, microscale dynamics study, and atom/ion trapping and cooling.

Funding. Advanced Research Projects Agency-Energy (DE-AR0000847); National Science Foundation (1541959).

Acknowledgment. S. W. D. L. acknowledges support from A*STAR Singapore through the National Science Scholarship Scheme. This work was performed in part at the Center for Nanoscale Systems (CNS), a member of the National Nanotechnology Coordinated Infrastructure Network (NNCI), which is supported by the NSF.

Disclosures. The authors declare no conflicts of interest.

Supplemental document. See Supplement 1 for supporting content.

†These authors contributed equally to this paper.

REFERENCES

1. A. Ashkin, "Acceleration and trapping of particles by radiation pressure," Phys. Rev. Lett. **24**, 156–159 (1970).
2. A. Ashkin, J. M. Dziedzic, J. E. Bjorkholm, and S. Chu, "Observation of a single-beam gradient force optical trap for dielectric particles," Opt. Lett. **11**, 288–290 (1986).
3. A. Ashkin and J. M. Dziedzic, "Optical trapping and manipulation of viruses and bacteria," Science **235**, 1517–1520 (1987).
4. O. M. Maragò, P. H. Jones, P. G. Gucciardi, G. Volpe, and A. C. Ferrari, "Optical trapping and manipulation of nanostructures," Nat. Nanotechnol. **8**, 807–819 (2013).
5. M. Daly, M. Sergides, and S. N. Chormaic, "Optical trapping and manipulation of micrometer and submicrometer particles," Laser Photon. Rev. **9**, 309–329 (2015).
6. T. D. Bouloumis and S. N. Chormaic, "From far-field to near-field micro- and nanoparticle optical trapping," Appl. Sci. **10**, 1375 (2020).
7. R. J. Niffenegger, J. Stuart, C. Sorace-Agaskar, D. Kharas, S. Bramhavar, C. D. Bruzewicz, W. Loh, R. T. Maxson, R. McConnell, D. Reens, G. N. West, J. M. Sage, and J. Chiaverini, "Integrated multi-wavelength control of an ion qubit," Nature **586**, 538–542 (2020).
8. P. L. Gould, P. D. Lett, P. S. Julienne, W. D. Phillips, H. R. Thorsheim, and J. Weiner, "Observation of associative ionization of ultracold laser-trapped sodium atoms," Phys. Rev. Lett. **60**, 788–791 (1988).
9. D. G. Grier, "A revolution in optical manipulation," Nature **424**, 810–816 (2003).
10. K. C. Neuman and S. M. Block, "Optical trapping," Rev. Sci. Instrum. **75**, 2787–2809 (2004).
11. K. Dholakia, P. Reece, and M. Gu, "Optical micromanipulation," Chem. Soc. Rev. **37**, 42–55 (2008).
12. H. Zhang and K. K. Liu, "Optical tweezers for single cells," J. R. Soc. Interface **5**, 671–690 (2008).
13. L. Mitchem and J. P. Reid, "Optical manipulation and characterisation of aerosol particles using a single-beam gradient force optical trap," Chem. Soc. Rev. **37**, 756–769 (2008).

14. K. Dholakia and T. Čižmár, "Shaping the future of manipulation," Nat. Photonics **5**, 335–342 (2011).
15. H. L. Guo and Z. Y. Li, "Optical tweezers technique and its applications," Sci. China Phys. Mech. Astron. **56**, 2351–2360 (2013).
16. A. Constable, J. Kim, J. Mervis, F. Zarinetchi, and M. Prentiss, "Demonstration of a-fiber-optical light-force trap," Opt. Lett. **18**, 1867–1869 (1993).
17. E. Sidick, S. D. Collins, and A. Knoesen, "Trapping forces in a multiple-beam fiber-optic trap," Appl. Opt. **36**, 6423–6433 (1997).
18. C. Liberale, P. Minzioni, F. Bragheri, F. De Angelis, E. Di Fabrizio, and I. Cristiani, "Miniaturized all-fibre probe for three-dimensional optical trapping and manipulation," Nat. Photonics **1**, 723–727 (2007).
19. Y. Liu and M. Yu, "Investigation of inclined dual-fiber optical tweezers for 3D manipulation and force sensing," Opt. Express **17**, 13624–13638 (2009).
20. C. Ti, M. T. Ho-Thanh, Q. Wen, and Y. Liu, "Objective-lens-free fiber-based position detection with nanometer resolution in a fiber optical trapping system," Sci. Rep. **7**, 13168 (2017).
21. H. Xin and B. Li, "Fiber-based optical trapping and manipulation," Front. Optoelectron. **12**, 97–110 (2019).
22. X. Zhao, N. Zhao, Y. Shi, H. Xin, and B. Li, "Optical fiber tweezers: A versatile tool for optical trapping and manipulation," Micromachines **11**, 114 (2020).
23. A. Asadollahbaik, S. Thiele, K. Weber, A. Kumar, J. Drozella, F. Sterl, A. M. Herkommer, H. Giessen, and J. Fick, "Highly efficient dual-fiber optical trapping with 3D printed diffractive fresnel lenses," ACS Photon. **7**, 88–97 (2020).
24. C. Liberale, G. Cojoc, F. Bragheri, P. Minzioni, G. Perozziello, R. La Rocca, L. Ferrara, V. Rajamanickam, E. Di Fabrizio, and I. Cristiani, "Integrated microfluidic device for single-cell trapping and spectroscopy," Sci. Rep. **3**, 01258 (2013).
25. S. Kawata and T. Tani, "Optically driven Mie particles in an evanescent field along a channeled waveguide," Opt. Lett. **21**, 1768–1770 (1996).
26. S. Gaugiran, S. Gétin, J. M. Fedeli, G. Colas, A. Fuchs, F. Chatelain, and J. Dérouard, "Optical manipulation of microparticles and cells on silicon nitride waveguides," Opt. Express **13**, 6956–6963 (2005).
27. A. H. J. Yang, T. Lerdsuchatawanich, and D. Erickson, "Forces and transport velocities for a particle in a slot waveguide," Nano Lett. **9**, 1182–1188 (2009).
28. B. S. Ahluwalia, P. McCourt, T. Huser, and O. G. Hellesø, "Optical trapping and propulsion of red blood cells on waveguide surfaces," Opt. Express **18**, 21053–21061 (2010).
29. H. Cai and A. W. Poon, "Optical trapping of microparticles using silicon nitride waveguide junctions and tapered-waveguide junctions on an optofluidic chip," Lab Chip **12**, 3803–3809 (2012).
30. S. H. Wu, N. Huang, E. Jaquay, and M. L. Povinelli, "Near-field, on-chip optical Brownian ratchets," Nano Lett. **16**, 5261–5266 (2016).
31. C. Pin, J. B. Jager, M. Tardif, E. Picard, E. Hadji, F. De Fornel, and B. Cluzel, "Optical tweezing using tunable optical lattices along a few-mode silicon waveguide," Lab Chip **18**, 1750–1757 (2018).
32. M. L. Juan, M. Righini, and R. Quidant, "Plasmon nano-optical tweezers," Nat. Photonics **5**, 349–356 (2011).
33. X. Yang, Y. Liu, R. F. Oulton, X. Yin, and X. Zhang, "Optical forces in hybrid plasmonic waveguides," Nano Lett. **11**, 321–328 (2011).
34. K. B. Crozier, "Quo vadis, plasmonic optical tweezers?" Light Sci. Appl. **8**, 35 (2019).
35. H. Tan, H. Hu, L. Huang, and K. Qian, "Plasmonic tweezers for optical manipulation and biomedical applications," Analyst **145**, 5699–5712 (2020).
36. Y. Y. Sun, X. C. Yuan, L. S. Ong, J. Bu, S. W. Zhu, and R. Liu, "Large-scale optical traps on a chip for optical sorting," Appl. Phys. Lett. **90**, 031107 (2007).
37. S. Lin, J. Hu, L. Kimerling, and K. Crozier, "Design of nanoslotted photonic crystal waveguide cavities for single nanoparticle trapping," Opt. Lett. **34**, 3451–3453 (2009).
38. S. Lin, E. Schonbrun, and K. Crozier, "Optical manipulation with planar silicon microring resonators," Nano Lett. **10**, 2408–2411 (2010).
39. S. Mandai, X. Serey, and D. Erickson, "Nanomanipulation using silicon photonic crystal resonators," Nano Lett. **10**, 99–104 (2010).
40. J. Hu, S. Lin, L. C. Kimerling, and K. Crozier, "Optical trapping of dielectric nanoparticles in resonant cavities," Phys. Rev. A **82**, 053819 (2010).
41. C. Renaut, B. Cluzel, J. Dellinger, L. Lalouat, E. Picard, D. Peyrade, E. Hadji, and F. De Fornel, "On chip shapeable optical tweezers," Sci. Rep. **3**, 2290 (2013).
42. A. Krishnan, N. Huang, S.-H. Wu, L. J. Martínez, and M. L. Povinelli, "Enhanced and selective optical trapping in a slot-graphite photonic crystal," Opt. Express **24**, 23271–23279 (2016).
43. S. Maruo, O. Nakamura, and S. Kawata, "Three-dimensional microfabrication with two-photon-absorbed photopolymerization," Opt. Lett. **22**, 132–134 (1997).
44. T. Gissibl, S. Thiele, A. Herkommer, and H. Giessen, "Two-photon direct laser writing of ultracompact multi-lens objectives," Nat. Photonics **10**, 554–560 (2016).
45. P.-I. Dietrich, M. Blaicher, I. Reuter, M. Billah, T. Hoose, A. Hofmann, C. Caer, R. Dangel, B. Offrein, U. Troppenz, M. Moehrle, W. Freude, and C. Koos, "In situ 3D nanoprinting of free-form coupling elements for hybrid photonic integration," Nat. Photonics **12**, 241–247 (2018).
46. S. Yu, H. Zuo, X. Sun, J. Liu, T. Gu, and J. Hu, "Optical free-form couplers for high-density integrated photonics (OFFCHIP): a universal optical interface," J. Lightwave Technol. **38**, 3358–3365 (2020).
47. S. Yu, X. Qiu, H. Zuo, M. Turduev, T. Gu, and J. Hu, "Compact and fabrication-tolerant waveguide bends based on quadratic reflectors," J. Lightwave Technol. **38**, 4368–4373 (2020).
48. T. Li, *Fundamental Tests of Physics with Optically Trapped Microspheres*, Springer Theses (Springer New York, 2013).
49. J. Kim and J. H. Shin, "Stable, free-space optical trapping and manipulation of sub-micron particles in an integrated microfluidic chip," Sci. Rep. **6**, 33842 (2016).
50. D. Michaelis, P. Schreiber, and A. Bräuer, "Cartesian oval representation of freeform optics in illumination systems," Opt. Lett. **36**, 918–920 (2011).
51. L. Liu, A. Woolf, A. W. Rodriguez, and F. Capasso, "Absolute position total internal reflection microscopy with an optical tweezer," Proc. Natl. Acad. Sci. USA **111**, E5609–E5615 (2014).